



Ground motion duration predictive models applicable for the Himalayan region

P ANBAZHAGAN^{1,*}  and KUNAL MOTWANI²

¹Department of Civil Engineering, Indian Institute of Science, Bangalore 560 012, India.

²Department of Civil Engineering, National Institute of Technology, Surathkal, Srinivasnagar, Mangalore 575 025, Karnataka, India.

*Corresponding author. e-mail: anbazhagan@iisc.ac.in

MS received 8 May 2021; revised 28 March 2023; accepted 29 March 2023

Several empirical models for the prediction of ground motion duration were developed across the world, but no model has been generated for the Himalayan region in the past. In this study, an attempt is made to study the duration models developed for different regions and compare them with a reference model developed for the Himalayan region for a wide range of magnitudes. The comparison is performed using the log-likelihood method and aims to identify the best duration prediction models based on the developed by Bajaj and Anbazhagan (2019) for the study region. The data support index values along with the weights of the corresponding models across the different distances and magnitude ranges have also been estimated. The study found that the predictive duration relation given by Lee and Green (2014) for Western North America is suitable for $M \leq 5$, while the model developed by Ghanat (2011) is suitable for $M > 5$ for the Himalayan region. The model developed by Afshari and Stewart (2016) is also very close to the reference model. It is always preferable to have a single duration predictive model for a wide range of magnitude and distance range; hence, there is a need to develop a region-specific duration predictive model for the Himalayan region.

Keywords. Duration; predictive equation; Himalayan region; log-likelihood method.

1. Introduction

The Himalayan region is regarded as one of the most seismically active regions globally. Nineteen thousand deaths in the great 1905 Kangra earthquake, loss of eleven thousand lives in the great 1934 Bihar earthquake (Auden and Ghosh 1934), and another thirty thousand casualties in the 1935 Quetta earthquake vividly remind us of the potential for great earthquake disaster in the shadows of the Himalayas (Khattri 1987). Earthquakes that occur in densely populated

mountainous regions, such as the Himalayas, have shown more significant earthquakes in the past due to a fast tectonic-plate collision. The high level of seismicity in the Himalayas is attributed to the collision of the Eurasian and the Indian tectonic plates 40 million years ago, leading to a rise of extensive folds and faults. The Indian plate was observed to be converging at a rate of 55 mm/year. Amongst this rate, a convergence of 22 mm/year was recorded by the Himalayas, while the remaining was accounted for by Tibet and Asia (Sharma *et al.* 2009; Ramkrishnan *et al.* 2019). The

Main Boundary Thrust (MBT), Main Central Thrust (MCT), and Main Frontal Thrust (MFT), formed due to the collision of the Indo-Eurasian tectonic plates, have attracted considerable interest from a large number of researchers worldwide. Even though this region is a highly earthquake-prone zone, no duration model has been generated for it in the past.

Currently, earthquake ground motions are usually characterized by peak ground acceleration and spectral ordinates. However, recent research investigations have revealed that the damage to a structure depends not only on these spectral parameters but also on the duration of ground motion (Yaghmaei-Sabegh *et al.* 2014). The duration of earthquake ground motion has also been shown to have significant effects on the extent of damage sustained by engineered structures during moderate to strong earthquakes. For two accelerograms of equal accelerations with different duration, the record with a longer duration would be more damaging, whereas, for two records with the same energy content, the record with a shorter duration would cause more damage (Bommer *et al.* 2009). Hence, the duration of earthquake ground motion should be considered an important parameter in addition to the amplitude and frequency content for adequately characterizing the effect of ground motion on seismic damage of structures.

Bommer *et al.* (2006) reviewed a large number of studies regarding ground motion duration. Inferences were made regarding the influence of duration on damage from a range of sources, including field studies of earthquakes, theoretical models of structural response, and experimental investigations. It was concluded that the influence of duration on a structure depends on several factors, such as the type of structure examined, the structural parameters used to quantify damage, and the other parameters used to characterize ground motion. The studies that consider hysteric energy loss find that the duration has an appreciable influence on the damage to the structures. In contrast, those studies that characterize damage by maximum response parameters find little or no impact on duration. The response of steel structures is expected to be far less sensitive to duration, whereas those structures whose strength deteriorates under the action of seismic shaking have a noticeable influence on duration.

This study compares various significant duration models developed for different regions with a reference model developed by Bajaj and Anbazhagan

(2019) for the Himalayan region. This comparison is performed by ranking various applicable duration models based on the log-likelihood values obtained through statistical analysis. The model with the highest rank for different magnitudes would be most accurate for estimating significant duration in the Himalayan region. Due to the lack of a large amount of ground motion duration data in the Himalayas, a duration model has not been developed in the past. Duration estimation can be performed more accurately if a regression model is developed using data from the Himalayas.

2. Seismotectonic of the study area

The entire Himalayan arc, 2500 km long, extending from Arunachal Pradesh in the northeast to Kashmir in the northwest, evolved as a result of the collision of the Indian and Asian continents about 50–60 million years ago. Over time, the sedimentary pile was completely folded. This, in turn, led to it being repeatedly split by faulting and thrusting. The Himalayan tectonic zone, being a collision plate boundary, is manifested with several north dipping thrusts that are exposed at the surface. These thrusts originate at a decollement surface dipping 15° from the south towards the north at depths ranging from about 12–20 km. These faults are the Trans-Himadri Fault (THF), the Main Central Thrust (MCT), the Main Boundary Thrust (MBT), and the Himalayan Frontal Thrust (HFT). The seismicity belt is mostly confined between Main Central Thrust (MCT) in the north and Main Boundary Thrust (MBT) in the south. It is relatively closer to the MCT. An outline map for the study region is shown in figure 1. The map also includes great earthquakes that have occurred in the past in this region. Anbazhagan *et al.* (2021) compiled 16 possible seismic sources capable of producing more significant earthquakes and estimated possible maximum and average amplification at 275 locations using site-specific deep shear wave velocity measured using passive and active seismic surface wave surveys. The study shows how different parts of North India are seismically hazardous due to future earthquakes and associated soil amplification. It is necessary to estimate the duration at different parts of the Himalayan region due to any future earthquake.

Anbazhagan *et al.* (2017) worked on developing empirical relationships for ground motion duration

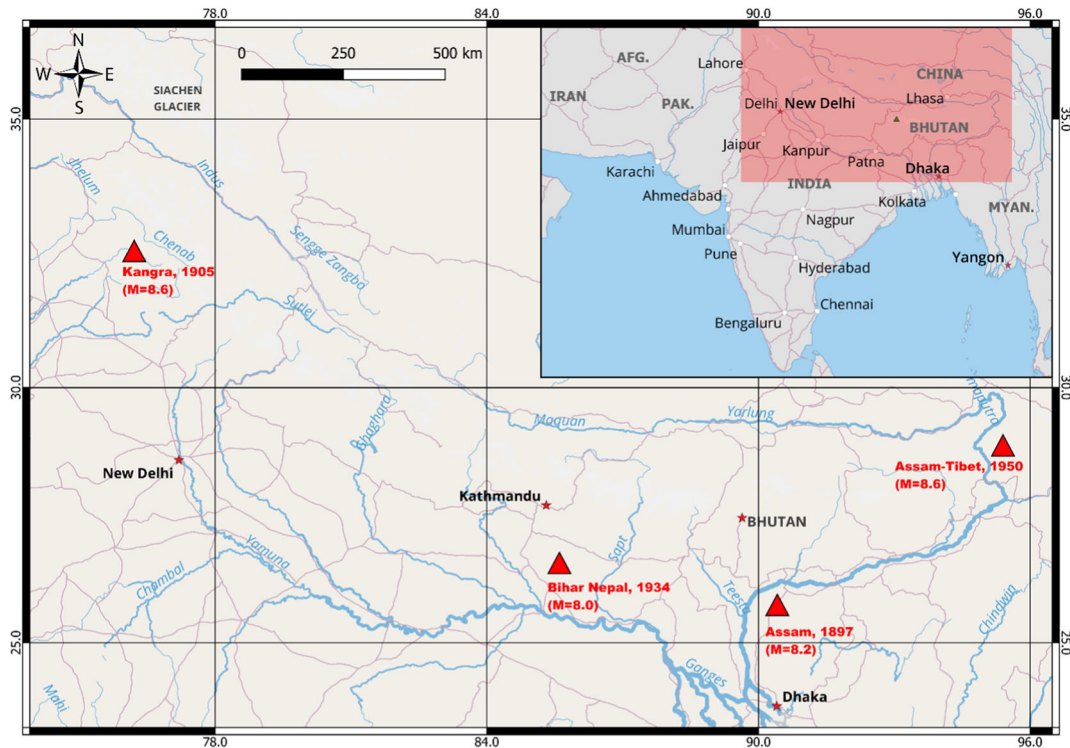


Figure 1. An outline map focusing on the Himalayan region, including historical great earthquakes that have occurred in this region in the past. The figure does not give a true representation of political borders and focuses on the distribution of the historical great earthquakes in the study area.

in the intraplate region using combined (Indian and other similar seismotectonic regions) intraplate earthquake data. However, very limited duration predictive relationships could be developed for the Himalayan region, due to the lack of a large amount of recorded ground motion data. Also, the role of Indian recorded data in the seismic duration predictive models on a global scale is very limited. For the first time, Bajaj and Anbazhagan (2019) developed a duration model using recorded earthquake data of 78 strong to moderate earthquakes that occurred in the Himalayan region from 1988 to 2015. The moment magnitude varied from 4.5 to 7.8, while the hypocentral distance ranged between 10 and 500 km. This model was developed for rock site conditions for the simulation of synthetic ground motions for the Himalayan region to develop a ground motion predictive equation applicable for a magnitude range of 4 to 9 and a distance of up to 750 km. However, there is no exclusive duration predictive model for the Himalayan region. Hence in this study, the duration model developed by Bajaj and Anbazhagan (2019) was used to identify the best suitable duration predictive models for the Himalayan region from the applicable duration predictive models.

3. Ground motion duration

A large number of definitions of strong-motion duration have been put forward by several researchers. However, these can generally be grouped into three generic categories, i.e., bracketed, uniform, and significant duration. Each of these definitions is based upon the fact that the damage potential of an earthquake is a function of the energy of the quake (Salmon *et al.* 1992; Bommer *et al.* 2006), and that the majority of the total energy associated with any earthquake is contained in portions of the earthquake time history which is much shorter in time than the entire duration (Bommer *et al.* 2006).

The first is the significant duration, which is defined as the interval between the times at which different values of Arias intensity are reached. Two generic measures of significant duration are the time intervals between 5–75% and 5–95% Arias intensity and are represented as D_{s5-75} and D_{s5-95} , respectively. D_{s5-75} intends to capture the energy from the body waves, whereas D_{s5-95} captures the energy from the full-wave train (Xie *et al.* 2012). The Arias intensity (AI) is defined as the time integral of the square of ground acceleration as per Arias (1970).

$$I_A = \frac{\pi}{2g} \int_0^t a^2(t) dt \quad (1)$$

where I_A represents the Arias intensity in m/s , $a(t)$ is the time acceleration history in m/s^2 , t is the total duration of the acceleration in seconds, and g is the acceleration due to gravity in m/s^2 . A plot of AI is called the Husid plot. Figure 2 shows the Husid plot of the 1991 Uttarkashi earthquake with markings of the time intervals between 5–75% and 5–95% energy. It can be noted here, that even though it would be expected that 5–75% energy should cover the entire body wave, we observe that this is not the case and instead the 5–95% energy covers the entire body and surface waves. The significant duration is useful as it reasonably helps in determining the duration of the most significant

shaking (Bommer and Martínez-Pereira 1999). We observe from figure 2 that the duration of the energy release from 5–95% was 13.56 seconds, while the duration for the final 5% is a little over 23 seconds.

Bracketed duration, D_B , is defined as the interval between the first and the last excursion of a specified threshold acceleration. Uniform duration, D_U , is similar to bracketed duration. However, in uniform duration, only those intervals are considered for which the ground acceleration is above the threshold. For this reason, D_B is always larger than D_U for a given record. Three threshold accelerations are used with each definition, these being 0.025, 0.05, and 0.10g, whence in total, six duration D_B (0.100g), D_B (0.050g), D_B (0.025g), D_U (0.100g), D_U (0.050g) and D_U (0.025g) definitions are

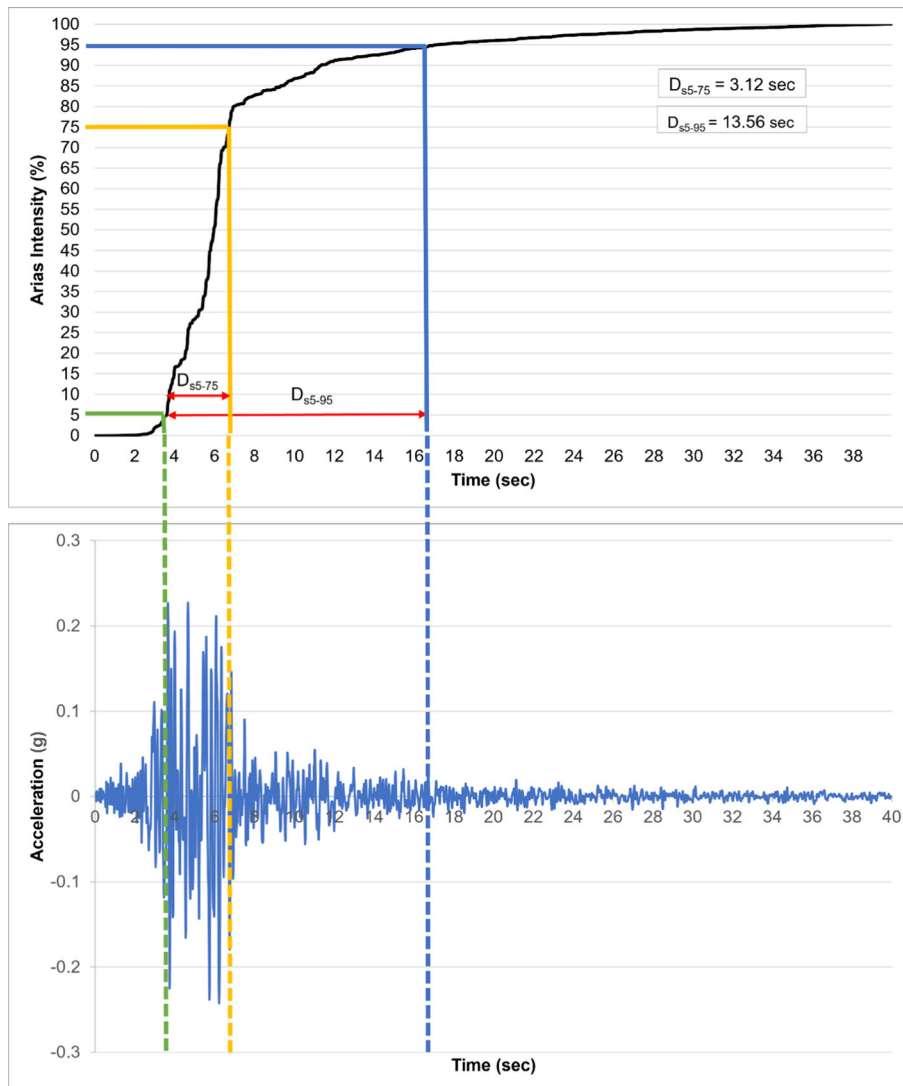


Figure 2. Husid plot for a significant duration of the 1991 Uttarkashi earthquake along with the corresponding time acceleration history of the region.

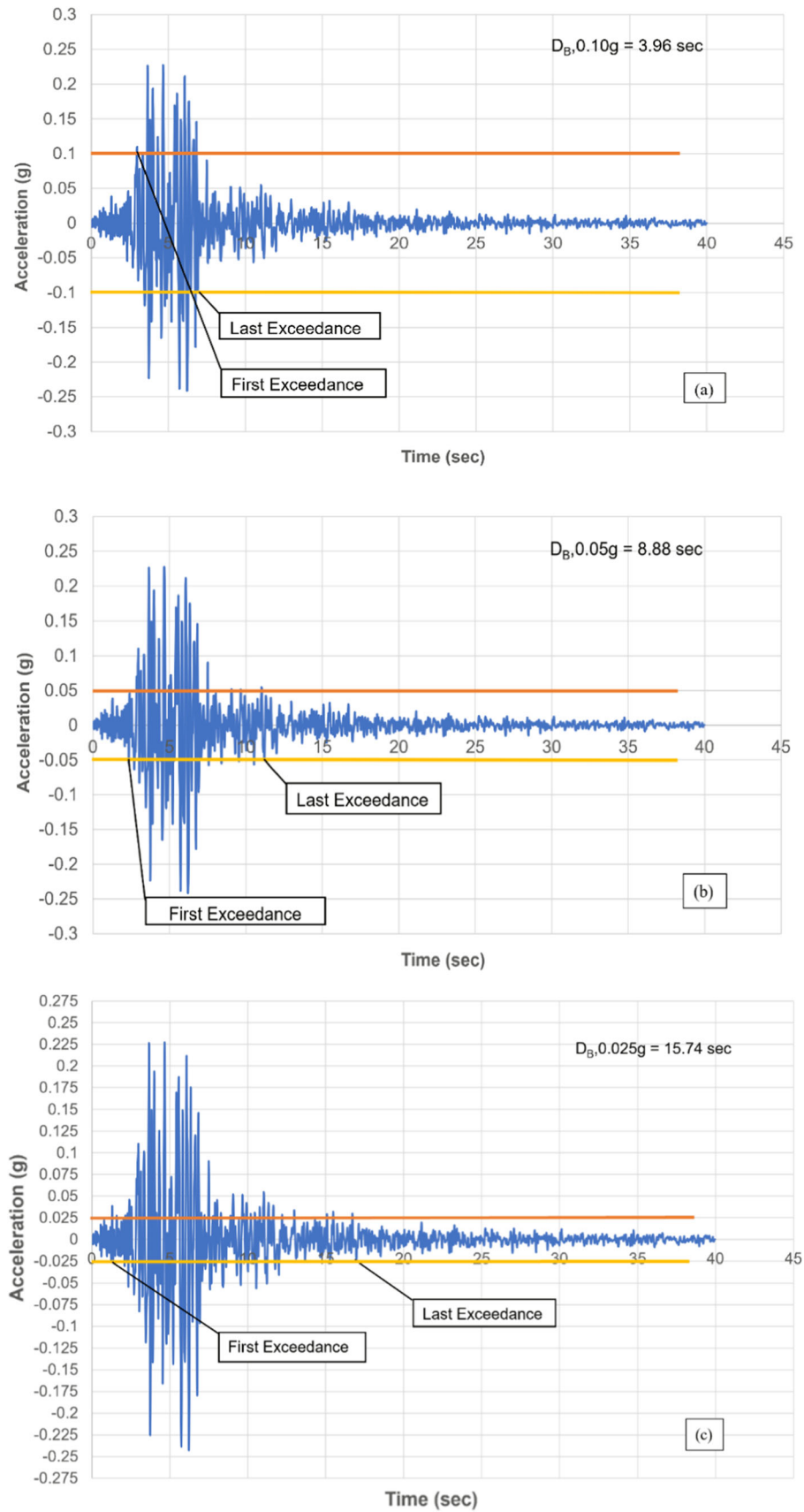


Figure 3. Bracketed duration of the 1991 Uttarkashi earthquake: (a) $D_B, 0.1g$, (b) $D_B, 0.05g$ and (c) $D_B, 0.025g$.

employed (Bommer *et al.* 2009). Figure 3(a–c) shows the 1991 Uttarkashi earthquake's bracketed duration for the considered threshold acceleration values. It is observed the value of D_B changes from 3.96 to 8.88 to 15.74 seconds as the threshold acceleration changes from $0.1g$ to $0.05g$ to $0.025g$. This clearly indicates that the bracketed duration is very sensitive to the threshold acceleration and small sub-event occurrences towards the end of a recording. For this reason, bracketed duration is not preferred.

Even though duration-related studies are significantly advanced in the world, minimal effort was made to understand different durations of Himalayan earthquakes and develop the region as a specific model for estimation of the same. Several duration predictive equations have been developed for interplate regions; however, very few have been developed for intraplate regions. Anbazhagan *et al.* (2017) developed the first duration model for the intraplate region, which included several datasets from the Indian region. The authors used data from 75 earthquakes from the intraplate regions from several locations of the globe, including Peninsular India. At the same time, there is no exclusive duration model which includes Indian active region earthquake data, so Bajaj and Anbazhagan (2019) used several parameters for the simulation of ground motion in the Himalayan region, one of them being the path duration function. The total duration was assumed to be the combination of the source duration and the path duration. However, due to a lack of a path duration model, authors developed a duration model part of the ground motion prediction equation development. The model used by Bajaj and Anbazhagan (2019) for calculating path duration used data from the entire Himalayan region for the rock site. It was noted that for smaller magnitudes, the input and output duration were almost similar. However, for a higher magnitude ($M > 5.5$) the output duration was approximately 0.94 of the input duration. The input duration was hence adjusted accordingly and the final model developed can be expressed as:

$$T_p = \begin{cases} R \times \frac{16.8}{60}, & R < 60 \text{ km} \\ 16.8 + 0.05 \times (R - 60), & R \geq 60 \text{ km}, \end{cases} \quad (2)$$

where R is the hypocentral distance.

Since there is no duration model for the Himalayan region, in this study, we use the above regional data-based model as reference model to compare similar seismotectonic duration predictive

models developed and identify duration models for future applications. About 16 duration predictive models were developed across the globe for varying magnitudes and are applicable to the Himalayan region. All details for these duration models are given by Douglas (2021). All the models used to calculate and compared in this study are for a significant duration of 5–95%.

The total duration is the combination of the source duration and the path duration. The source duration is assumed to be the reciprocal of corner frequency, while the path duration relates to the propagation effects and other effects related to the site and complex source effects. Thus, the source duration is subtracted from the total duration to estimate the path duration. Bajaj and Anbazhagan (2019) have developed the duration model using either acceleration or velocity database using effective duration (D'_{95}) as described in Boore and Thompson (2014) and it stated that the simulations of effective duration could be compared in terms of total duration. Since the variation is uniform and can be compared, we conclude that comparing the path duration with significant duration will not affect the comparison. Further, the path duration equation specified by Bajaj and Anbazhagan (2019) is based on 5 to 95% of AI, so it is similar to the significant duration in the other papers. A report generated by Douglas (2021) summarizes all the predictive equations developed in Engineering Seismology from 1963. Duration predictive models for a significant duration of 5 to 95% are considered in this study. A table was also provided in the report to include the general characteristics of these empirical equations for the prediction of duration and summarized a number of models for a relatively significant duration. The predictive duration equation considered in this study is outlined in table 1.

4. Analysis of duration predictive equations

Simple duration predictive models are a function of magnitude and hypocentral distance, whereas some complex models need fault rupture parameters and site conditions to determine duration. A summary of duration models considered in the study, along with their regression coefficients, is given in table 1. An increasing number of duration models necessitates a structured, quantifiable, and robust technique to select and rank different models for the Himalayan region. It is significant to select an

Table 1. Summary of available models for the duration of ground motion.

Sl. no.	Reference	Abbreviation of expression	Duration equation	Magnitude range (M)	Distance range (km)
1	Trifunac and Brady (1975)	TRBR-75	$D = as + bM + cR \pm \sigma$	3.8–7.7	6–400
2	Dobry et al. (1978)	DO-78	$\log D = 0.43M - 1.83$	4.7–7.6	0.1–130
3	Kamiyama (1984)	KA-84	$t_p = 0.44 \times 10^{0.21M} \times \Delta^{0.048} \times 10^{-0.0019H} \times (1.83C_{du} + 0.6)$	4.1–7.9	10–310
4	Abrahamson and Silva (1996)	ABSI-96	$\ln(D_{0.05-0.95}) = a_1 + a_2 \ln\left(\frac{0.9}{0.05}\right) + a_3 \left(\ln\left(\frac{0.9}{0.05}\right)\right)^2 + \ln\left[\frac{((\Delta\sigma/10^{1.5M+16.05})^{-1/3})}{4.9 \times 10^{\beta}} + S_{c1} + c_2(R - 10)\right]$	4.7–7.4	0.1–220
5	Hernandez and Cotton (2000)	HECO-00	$\log D = a + bM + c \log(R) + dS \pm \sigma$	3.2–7.4	1–109
6	Kempton and Stewart (2006)	KEST-06	$\ln SD = \ln\left[\frac{((\Delta\sigma/10^{1.5M+16.05})^{-1/3})}{4.9 \times 10^{\beta}}\right] c_1 S + c_2(R) \pm \sigma$	5–7.6	0–200
7	Pousse et al. (2006)	PO-06	$\log_{10}(SD) = aM + b \log_{10}(R) + S_k$	4.1–7.3	5–250
8	Snæbjörnsson and Sighjörnsson (2008)	SNSI-08	$\log_{10}(\tau_{sr}) = b_1 + b_2 M_w + b_3 \log_{10} \sqrt{d^2 + b_4^2}$	5–7.6	0–100
9	Bommer et al. (2009)	BO-09	$\ln D = c_0 + m_1 M + (r_1 + r_2 M) \ln \sqrt{R_{rup}^2 + h_1^2} + v_1 \ln V_{s30} + z_1 Z_{top}$	4.8–7.9	1.5–100
10	Ghanat (2011)	GH-11	$\ln(SD) = \{(c_0 + c_1(M - 6)) + (c_2 + c_3(R_{rup})) + (c_4 + c_5(V_{s30}))\} + \varepsilon$	4.8–7.9	0.2–200
11	Lee and Green (2014) (CENA)	LGCE-14	$\ln D_{5-95} = \ln\{c_1 + c_2 \exp(M - 6) + c_3 R + [S_1 + S_2(M - 6) + S_3 R] S_s\}$	5–7.6	0.1–199.1
12	Lee and Green (2014) (WNA)	LGWN-14	$\ln D_{5-95} = \ln\{c_1 + c_2 \exp(M - 6) + c_3 R + [S_1 + S_2(M - 6) + S_3 R] S_s\}$	5–7.6	0.1–199.1
13	Yaghmaei-Sabegh et al. (2014)	YASA-14	$\log(D_a) = (a_1 + a_2 \log(R))^{b_1} + a_3 M^{b_2} + a_4 S + \eta + \varepsilon$	3.7–7.7	0.6–294
14	Afshari and Stewart (2016)	AFST-16	$\ln D = \ln(F_E(M, mech) + F_P(R_{rup})) + F_S(V_{s30}, \delta_{z_1}) + \varepsilon_p \sigma(M)$	3.0–7.9	0–300
15	Sandikhayya and Akkar (2016)	SAAK-16	$\ln SD = \left\{ a_1 + a_2(M_w - 6.5) + a_3(8.5 - M_w)^2 + [a_4 + a_5(M_w - 6.5)] \ln\left(\sqrt{R^2 + a_6^2}\right) + a_7 F_N + a_8 F_R + a_9 \ln\left[\frac{\min(V_{s30}, 1000)}{750}\right] + \varepsilon \sigma \right\}$	4.0–7.6	0–200
16	Podili and Raghukanth (2019)	PORA-19	$\ln(T_{sig}) = d_0 + f(M_w) + d_6 b + S_c + S_s + d_f F_M + d_r R + d_8 \ln(R + d_9 \exp(d_{10} M_w)) + d_{6s} R + d_{11} \ln(V_{s30}) + d_{12} L_{arc} R + \sigma$	5.0–9.0	5–350
17	Huang et al. (2020)	HU-20	$\log(D) = b_1 + b_2 M + b_3 M^2 + (b_4 + b_5 M) \log\left(\sqrt{R^2 + b_6^2}\right) + b_7 S_s + b_8 S_A + b_9 F_N + b_{10} F_R + \eta + \varepsilon$	4–6.5	1–220

Table 1. (Continued.)

Sl. no.	Study region	Number of accelerogram records	Symbol abbreviation	Constants
1	Western USA	188	M – Moment magnitude; R – Hypocentral distance	$a = -4.88, b = 2.33, c = 0.149, \sigma = 10.67$
2	Western USA	84	M – Moment magnitude	
3	Japan	192	M – Moment magnitude; Δ – Site to source distance;	$H = 80, C_{du} = 0$
4	Worldwide data from shallow crustal events near active plate margins	853	H – Depth of hypocenter; C_{du} – duration coefficient $\Delta\sigma$ – Stress drop; M – Moment magnitude; R – Hypocentral distance	$a_1 = -0.532 \pm 0.005, a_2 = 0.552 \pm 0.002,$ $a_3 = -0.0262 \pm 0.0013, b_1 = 5.204 \pm 0.105,$ $b_2 = 0.851 \pm 0.146, c_1 = 0.805, c_2 = 0.063,$ $\beta = 3.2$
5	163 Records from California and 109 from Italy	272	M – Moment magnitude; R – Hypocentral distance	$a = -1.04, b = 0.44, c = 0.19, d = 0.04, \sigma = 0.48,$ $S = 0$
6	Worldwide data from shallow crustal events near active plate margins	1559	$\Delta\sigma$ – Stress drop; β – Shear wave velocity; M – Moment magnitude; R – Hypocentral distance	$\Delta\sigma = 24 \pm 9, c_1 = 1.91 \pm 0.5, c_2 = 0.15 \pm 0.02,$ $\beta = 3.2, \sigma = 0.51, S = 0$
7	Japan	9390	M – Moment magnitude; R – Hypocentral distance; S – Soil site coefficient	$a = 0.05793, b = 0.2658, s_k = -0.2437$
8	Europe and Middle East	71	M_w – Moment magnitude;	$b_1 = -1.3877, b_2 = 0.2451,$
9	Worldwide data from shallow crustal events near active plate margins	2409	d – Distance to surface trace of the fault	$b_3 = 0.6280, b_4 = 4.50, \sigma = 0.1663$
			M – Moment magnitude; R_{rup} – Fault rupture distance; Z_{tor} – Depth to top of rupture;	$c_0 = -2.393 \pm 0.8051, m_1 = 0.9368 \pm 0.1223,$
			V_{s30} – Average shear wave velocity	$r_1 = 1.5686 \pm 0.1489, r_2 = -0.1953 \pm 0.0219,$
				$h_1 = 2.5, v_1 = -0.3478 \pm 0.0274,$ $z_1 = -0.0365 \pm 0.0202$
10	Worldwide data from shallow crustal events near active plate margins	3551	M – Moment magnitude; R_{rup} – Fault rupture distance; V_{s30} – Average shear wave velocity; ϵ – Residual error	$c_0 = 1.5424129, c_1 = 0.614659, c_2 = -0.332157,$ $c_3 = 0.011385, c_4 = 0, c_5 = -0.00048$

Table 1. (Continued.)

Sl. no.	Study region	Number of accelerogram records	Symbol abbreviation	Constants
11	Central and Eastern North America	324	M – Moment magnitude; R – Closest distance to rupture faults	$c_1 = 2.5$, $c_2 = 0.21$, $c_3 = 2.14$, $S_1 = -0.98$, $S_2 = -0.45$, $S_3 = -0.0071$, $S_8 = 0.00$
12	Western North America	324	M – Moment magnitude; R – Closest distance to rupture faults	$c_1 = 1.5$, $c_2 = 3.22$, $c_3 = 0.11$, $S_1 = 2.01$, $S_2 = 0.8$, $S_8 = -0.0097$, $S_8 = 0.00$
13	Iran	286	R – Hypocentral distance; M – Moment magnitude; S – Site condition	$a_0 = 0.271 \pm 0.12$, $a_1 = 0.07$, $a_2 = 0.236$, $a_3 = 0.16 \pm 0.01$, $a_4 = -0.021 \pm 0.011$, $b_1 = 1.24$, $b_2 = 1.02$, $\sigma = 0.313$
14	Worldwide data from shallow crustal events near active plate margins	11195	F_P – Source duration; F_R – Path duration; F_s – Site term; V_{s30} – Average shear wave velocity; ε_n – Standard normal variate	$M_1 = 5.2$, $M_2 = 7.4$, $b_0 = 2.182$, $b_1 = 3.628$, $b_2 = 0.9443$, $b_3 = -3.911$, $c_1 = 0.3165$, $c_2 = 0.2539$, $c_3 = 0.0932$, $R_1 = 10$, $R_2 = 50$, $V_1 = 600$, $V_{ref} = 369.9$
15	Europe and Middle East	1041	M_w – Moment magnitude; R – Hypocentral distance; F_N and F_R – the amplitude difference due to different types of faulting; V_{s30} – Shear wave velocity up to 30 meters	$a_1 = 1.11533$, $a_2 = 1.24873$, $a_3 = 0.04921$, $a_4 = 0.38781$, $a_5 = -0.19161$, $a_6 = 7.5$, $a_7 = 0.06962$, $a_8 = -0.18352$, $a_9 = -0.2957$, $\sigma = 0.49049$
16	Japan	96880	M_w – Moment magnitude; R – Hypocentral distance; S_c and S_s – Source constants; V_{s30} – Shear wave velocity up to 30 meters	$d_0 = -3.717$, $d_1 = 0.035$, $d_2 = 0.085$, $d_3 = -0.041$, $d_4 = 17.06$, $d_5 = -134.0$, $d_6 = 0$, $S_c = 4.258$, $S_s = 4.125$, $d_f = 0.032$, $d_7 = -0.001$, $d_8 = 0.735$, $d_9 = 0.0086$, $d_{10} = 1.014$, $d_{s_s} = 0.035$, $d_{11} = -0.148$, $d_{12} = 0.007$, $\sigma_{intra} = 0.372$, $\sigma_{inter} = 0.277$, $\sigma(\varepsilon) = 0.464$
17	Italy	5703	M – Moment magnitude; R – Hypocentral distance; S_A and S_s – Site variables; F_N and F_R – Site variables	$b_1 = -0.555$, $b_2 = -0.092$, $b_3 = 0.035$, $b_4 = 1.343$, $b_5 = -0.111$, $b_6 = 8.404$, $b_7 = 0.091$, $b_8 = 0.015$, $b_9 = 0.024$, $b_{10} = 0.036$, $\tau = 0.063$, $\Phi = 0.187$

appropriate model to predict ground motion duration in the region where no such model was developed, as it is a crucial element in seismic hazard analysis. In the past, comparisons between various models were performed using the efficacy test. Efficacy tests can be performed for quantitative assessments of numerous models. This test makes use of the average sample log-likelihood (LLH) method for ranking purposes.

LLH method is based on the log-likelihood approach, which measures the distance between two continuous probability density functions $f(x)$ and $g(x)$. The distribution of an observed data point is represented by the function $f(x)$, whereas the distribution of the estimated data point is represented by the function $g(x)$ (Scherbaum *et al.* 2009; Anbazhagan *et al.* 2016). This approach calculates the average log-likelihood of the predictive model considered using the data of the observed model to obtain a model selection index. The LLH value is calculated by

$$\text{LLH}(g, x) = -\frac{1}{N} \sum_{i=1}^N \log_2(g(x_i)) \quad (3)$$

where x_i represents the observed data for $i = 1$ through N . The variable N represents the total number of data points. A smaller LLH value indicates a better relationship between the observed and the estimated ground motion data. In this study, the LLH approach is used to measure the distance between the reference model developed by Bajaj and Anbazhagan (2019) and the duration models developed for regions across the globe. The LLH values can then be used to estimate the LLH-based weights for each model using the below equation stated in Delavaud *et al.* (2012).

$$w_i = \frac{2^{-\text{LLH}(g_i, x)}}{\sum_{k=1}^n 2^{-\text{LLH}(g_k, x)}} \quad (4)$$

The LLH-based weight gives an indication to what degree data increases or decreases the weight of the model with respect to the state of non-informativeness (Delavaud *et al.* 2012). Delavaud also proposed another parameter called Data Support Index (DSI) which estimates the degree to which the data supports or rejects a model with respect to the state of non-informativeness. DSI can be estimated using the equation:

$$\text{DSI} = 100 \times \frac{w_i - w_{\text{unif}}}{w_{\text{unif}}} \quad (5)$$

where w_i is the LLH-based weight and $w_{\text{unif}} = 1/M$ and M represents the number of duration predictive models used during LLH calculation. A positive DSI value shows that the duration model supports the reference model whereas a negative DSI value rejects the model. In the present study, LLH-based weights are initially estimated to determine if the DSI value for a model is positive or negative. The models having negative DSI values are then rejected, and revised weights are estimated for the models with positive DSI.

5. LLH analysis and discussion

Ranking of the duration models not only provides the best model but also helps in predicting reliable duration for potential future earthquakes. In this study, different duration models are ranked based on log-likelihood values. Three different ranges of hypocentral distance are considered for this study, i.e., segmented analysis as per Anbazhagan *et al.* (2016). The three ranges are 0–150, 150–300, and 300–450 km, respectively. Since an accurate duration equation has not been developed in the past for the Himalayan region, the applicable magnitude and distance range cannot be predicted if the total distance is used. In the interest of an engineering hypothesis, it is assumed that all equations compared to the reference equation are within the prescribed range for magnitude and distance. Using this presumption, the analytical correlation has been further studied. Graphically comparing each model could give debatable results, and hence the log-likelihood value is calculated to provide quantitative values. Log-likelihood values are calculated for the three ranges of hypocentral distance for a magnitude ranging from 4.0–8.0. Table 2 represents these log-likelihood values along with their corresponding ranks, DSI value, and LLH-based weight. The number of times the LLH rank is repeated within a threshold value is also noted. We have considered 3 threshold values in this study, i.e., 3, 5, and 10. Since 3 hypocentral distance ranges are considered, we have chosen the least threshold value as 3. It was noticed that the LLH values were lower for a hypocentral distance of 0–150 km and increased as the distance increased for most cases. A graphical comparison of different models is shown in figure 4 for a magnitude of 6.5 in the 0–150 km range. Models with LLH ranks of eight and above have been excluded from this figure.

Table 2. Ranking of models based on LLH criteria for varying ranges of hypocentral distances for magnitudes 4.0, 5.0, 6.5, 7.0 and 8.0. The DSI values and weights for each corresponding model has also been estimated. The abbreviation UD stands for ‘undetectable’, VH stands for ‘very high’ and NA stands for ‘not applicable’.

Duration model	Magnitude 4															
	0–150 km					150–300 km					300–450 km					
	LLH	Rank	DSI	Weight	LLH	Rank	DSI	Weight	LLH	Rank	DSI	Weight	LLH	Rank	DSI	Weight
TRBR-75	2.124	4	66.39	0.14	3.996	7	-49.45	NA	9.28	7	-96.60	NA	9.28	7	-96.60	NA
DO-78	UD	VH	-	-	UD	VH	-	-	UD	VH	-	-	UD	VH	-	-
KA-84	UD	VH	-	-	UD	VH	-	-	UD	VH	-	-	UD	VH	-	-
ABSI-96	2.412	6	36.28	0.11	2.612	5	31.92	0.13	6.639	6	-78.76	NA	6.639	6	-78.76	NA
HECO-00	UD	VH	-	-	UD	VH	-	-	UD	VH	-	-	UD	VH	-	-
KEST-06	1.839	2	102.74	0.17	2.4081	4	51.95	0.15	6.111	5	-69.38	NA	6.111	5	-69.38	NA
PO-06	25.17	12	-100.00	NA	UD	VH	-	-	UD	VH	-	-	UD	VH	-	-
SNSI-08	7.604	10	-96.27	NA	37.726	11	-100.00	NA	70.741	11	-100.00	NA	70.741	11	-100.00	NA
BO-09	3.853	9	-49.81	NA	6.373	9	-90.27	NA	10.707	8	-98.73	NA	10.707	8	-98.73	NA
GH-11	23.892	11	-100.00	NA	3.034	6	-1.53	NA	2.356	1	313.43	0.38	2.356	1	313.43	0.38
LGWN-14	1.836	1	103.16	0.17	1.496	2	185.94	0.28	2.879	3	187.71	0.26	2.879	3	187.71	0.26
LGCE-14	2.131	5	65.59	0.14	2.279	3	66.18	0.16	5.67	4	-58.43	NA	5.67	4	-58.43	NA
YASA-14	3.797	8	-47.82	NA	25.059	10	-100.00	NA	55.397	10	-100.00	NA	55.397	10	-100.00	NA
AFST-16	1.846	3	101.75	0.17	1.451	1	195.00	0.29	2.401	2	300.73	0.36	2.401	2	300.73	0.36
SAAK-16	UD	VH	-	-	UD	VH	-	-	UD	VH	-	-	UD	VH	-	-
PORA-19	80.944	13	-100.00	NA	159.812	12	-100.00	NA	238.63	12	-100.00	NA	238.63	12	-100.00	NA
HU-20	2.62	7	17.98	0.10	6.296	8	-89.74	NA	16.393	9	-99.98	NA	16.393	9	-99.98	NA

Duration model	Magnitude 5															
	0–150 km					150–300 km					300–450 km					
	LLH	Rank	DSI	Weight	LLH	Rank	DSI	Weight	LLH	Rank	DSI	Weight	LLH	Rank	DSI	Weight
TRBR-75	2.37	6	29.35	0.11	4.627	8	-72.56	NA	10.382	8	-98.61	NA	10.382	8	-98.61	NA
DO-78	UD	VH	-	-	UD	VH	-	-	UD	VH	-	-	UD	VH	-	-
KA-84	UD	VH	-	-	UD	VH	-	-	UD	VH	-	-	UD	VH	-	-
ABSI-96	2.308	5	35.03	0.11	2.961	7	-12.93	NA	7.538	7	-90.03	NA	7.538	7	-90.03	NA
HECO-00	UD	VH	-	-	UD	VH	-	-	UD	VH	-	-	UD	VH	-	-
KEST-06	1.827	2	88.46	0.15	2.572	6	14.02	0.11	6.491	6	-79.40	NA	6.491	6	-79.40	NA
PO-06	17.304	12	-100.00	NA	UD	VH	-	-	UD	VH	-	-	UD	VH	-	-
SNSI-08	2.382	7	28.28	0.10	2.153	4	52.44	0.14	2.37	1	258.42	0.31	2.37	1	258.42	0.31
BO-09	3.952	9	-56.79	NA	7.7	10	-96.74	NA	14.962	9	-99.94	NA	14.962	9	-99.94	NA
GH-11	7.357	11	-95.92	NA	1.753	3	101.15	0.19	3.127	4	112.09	0.19	3.127	4	112.09	0.19
LGWN-14	1.825	1	88.72	0.15	1.534	2	134.12	0.22	3.086	3	118.20	0.19	3.086	3	118.20	0.19
LGCE-14	2.051	4	61.36	0.13	2.431	5	25.72	0.12	6.025	5	-71.55	NA	6.025	5	-71.55	NA
YASA-14	4.624	10	-72.88	NA	37.303	11	-100.00	NA	90.811	11	-100.00	NA	90.811	11	-100.00	NA

Table 2. (Continued.)

Duration model	Magnitude 5												Number of repeated within rank of			
	0–150 km				150–300 km				300–450 km							
	LLH	Rank	DSI	Weight	LLH	Rank	DSI	Weight	LLH	Rank	DSI	Weight		3	5	10
AFST-16	1.846	3	86.00	0.15	1.451	1	147.99	0.23	2.401	2	250.81	0.31	3	3	3	
SAAK-16	UD	VH	-	-	UD	VH	-	-	UD	VH	-	-	-	-	-	
PORA-19	81.473	13	-100.00	NA	160.29	12	-100.00	NA	239.108	12	-100.00	NA	-	-	-	
HU-20	2.625	8	8.39	0.09	6.643	9	-93.22	NA	17.537	10	-99.99	NA	-	-	3	
Magnitude 6.5																
Duration model	0–150 km				150–300 km				300–450 km				Number of repeated within rank of			
	LLH	Rank	DSI	Weight	LLH	Rank	DSI	Weight	LLH	Rank	DSI	Weight	3	5	10	
TRBR-75	2.878	7	-7.74	NA	5.712	7	-71.03	NA	12.172	7	-98.74	NA	-	-	3	
DO-78	UD	VH	-	-	UD	VH	-	-	UD	VH	-	-	-	-	-	
KA-84	UD	VH	-	-	UD	VH	-	-	UD	VH	-	-	-	-	-	
ABSI-96	3.746	10	-49.45	NA	7.413	9	-91.09	NA	15.715	9	-99.89	NA	-	-	3	
HECO-00	3.272	9	-29.79	NA	3.778	5	10.69	0.09	5.263	4	51.24	0.12	-	2	3	
KEST-06	2.149	6	52.93	0.14	4.086	6	-10.59	NA	9.461	6	-91.76	NA	-	-	3	
PO-06	9.664	13	-99.16	NA	172.243	14	-100.00	NA	UD	VH	-	-	-	-	-	
SNSI-08	2.127	5	55.28	0.14	5.907	8	-74.70	NA	15.33	8	-99.86	NA	-	1	3	
BO-09	4.614	11	-72.30	NA	17.777	11	-99.99	NA	44.53	11	-100.00	NA	-	-	-	
GH-11	1.529	1	135.03	0.22	2.42	3	183.72	0.23	3.638	1	366.48	0.37	3	3	3	
LGWN-14	2.028	4	66.31	0.16	1.994	1	281.18	0.31	4.472	3	161.68	0.21	2	3	3	
LGCE-14	1.865	2	86.20	0.17	3.53	4	31.45	0.11	8.245	5	-80.86	NA	1	3	3	
YASA-14	6.019	12	-89.54	NA	57.115	12	-100.00	NA	150.31	12	-100.00	NA	-	-	-	
AFST-16	1.937	3	77.13	0.17	2.16	2	239.75	0.27	3.89	2	291.72	0.31	3	3	3	
SAAK-16	UD	VH	-	-	UD	VH	-	-	UD	VH	-	-	-	-	-	
PORA-19	84.084	14	-100.00	NA	162.901	13	-100.00	NA	241.719	13	-100.00	NA	-	-	-	
HU-20	3.175	8	-24.90	NA	11.257	10	-99.38	NA	29.479	10	-100.00	NA	-	-	3	
Magnitude 7																
Duration model	0–150 km				150–300 km				300–450 km				Number of repeated within rank of			
	LLH	Rank	DSI	Weight	LLH	Rank	DSI	Weight	LLH	Rank	DSI	Weight	3	5	10	
TRBR-75	3.085	6	9.77	0.09	6.11	5	-55.42	0	12.805	5	-97.64	0.00	-	2	3	
DO-78	UD	VH	-	-	UD	VH	-	-	UD	VH	-	-	-	-	-	
KA-84	UD	VH	-	-	UD	VH	-	-	UD	VH	-	-	-	-	-	
ABSI-96	8.547	13	-97.51	NA	14.993	9	-99.90	NA	26.82	9	-100.00	NA	-	-	2	
HECO-00	4.269	9	-51.69	NA	17.081	10	-99.97	NA	15.224	7	-99.56	NA	-	-	3	

Table 2. (Continued.)

Duration model	Magnitude 7												Number of repeated within rank of		
	0-150 km				150-300 km				300-450 km						
	LLH	Rank	DSI	Weight	LLH	Rank	DSI	Weight	LLH	Rank	DSI	Weight	3	5	10
KEST-06	3.1	7	8.63	0.09	6.166	6	-57.11	NA	12.919	6	-97.82	NA	-	-	3
PO-06	7.935	12	-96.19	NA	135.254	13	-100.00	NA	UD	VH	-	-	-	-	-
SNSI-08	2.475	5	67.53	0.14	8.702	7	-92.60	NA	22.827	8	-100.00	NA	-	1	3
BO-09	5.622	10	-81.09	NA	34.424	11	-100.00	NA	91.947	11	-100.00	NA	-	-	1
GH-11	2.06	2	123.37	0.18	3.37	3	197.81	0.23	4.793	1	508.83	0.49	3	3	3
LGWN-14	2.209	4	101.45	0.16	2.704	1	372.53	0.36	5.954	3	172.27	0.22	2	3	3
LGCE-14	2.035	1	127.27	0.18	4.014	4	90.58	0.15	8.66	4	-58.27	NA	1	3	3
YASA-14	6.444	11	-89.30	NA	63.936	12	-100.00	NA	171.12	12	-100.00	NA	-	-	-
AFST-16	2.208	3	101.59	0.16	3.162	2	244.01	0.26	5.503	2	272.19	0.30	3	3	3
SAAK-16	UD	VH	-	-	UD	VH	-	-	UD	VH	-	-	-	-	-
PORA-19	86.237	14	-100.00	NA	165.054	14	-100.00	NA	243.872	13	-100.00	NA	-	-	-
HU-20	3.612	8	-23.82	NA	14.985	8	-99.90	NA	39.171	10	-100.00	NA	-	-	3

Duration model	Magnitude 8												Number of repeated within rank of		
	0-150 km				150-300 km				300-450 km						
	LLH	Rank	DSI	Weight	LLH	Rank	DSI	Weight	LLH	Rank	DSI	Weight	3	5	10
TRBR-75	3.552	4	87.10	0.15	6.962	3	-18.86	NA	14.128	3	-98.33	NA	2	3	3
DO-78	UD	VH	-	-	UD	VH	-	-	UD	VH	-	-	-	-	-
KA-84	80.955	12	-100.00	NA	UD	VH	-	-	UD	VH	-	-	-	-	-
ABSI-96	81.378	13	-100.00	NA	100.465	12	-100.00	NA	129.71	10	-100.00	NA	-	-	1
HECO-00	6.643	8	-78.04	NA	59.316	9	-100.00	NA	120.053	9	-100.00	NA	-	-	3
KEST-06	17.037	11	-99.98	NA	25.68	7	-100.00	NA	39.241	7	-100.00	NA	-	-	2
PO-06	5.378	6	-47.23	NA	79.75	11	-100.00	NA	UD	VH	-	-	-	-	1
SNSI-08	3.197	3	139.30	0.20	13.481	5	-99.12	NA	35.262	6	-100.00	NA	1	2	3
BO-09	UD	VH	-	-	UD	VH	-	-	UD	VH	-	-	-	-	-
GH-11	2.289	1	349.03	0.37	3.636	1	713.65	0.68	4.971	1	855.33	0.87	3	3	3
LGWN-14	8.44	10	-93.68	NA	9.268	4	-83.59	NA	15.895	4	-99.51	NA	-	2	3
LGCE-14	6.242	7	-71.01	NA	13.955	6	-99.36	NA	23.693	5	-100.00	NA	-	1	3
YASA-14	7.157	9	-84.62	NA	71.492	10	-100.00	NA	194.249	11	-100.00	NA	-	-	2
AFST-16	2.707	2	236.08	0.28	4.707	2	287.29	0.32	7.716	2	42.50	0.13	3	3	3
SAAK-16	UD	VH	-	-	UD	VH	-	-	UD	VH	-	-	-	-	-
PORA-19	100.58	14	-100.00	NA	179.399	13	-100.00	NA	UD	VH	-	-	-	-	-
HU-20	5.121	5	-36.94	NA	29.145	8	-100.00	NA	76.728	8	-100.00	NA	-	1	3

In the 0–150 km range, the model developed by Kempton and Stewart (2006) has low log-likelihood values for magnitudes up to seven. However, for moment magnitudes of seven and above, this model may not give accurate values for the duration in the Himalayan region. The models developed by Kamiyama (1984), Dobry *et al.* (1978) and Sandikkaya and Akkar (2016) have very high LLH values and are hence not suitable. It was not possible to calculate the exact LLH values for these models as the normal distribution value for these points tends to be zero. Since the LLH value could not be determined, the weights and, ultimately the DSI value could also not be estimated. The model

developed by Podili and Raghukanth (2019) also has very high LLH values and is hence not suitable. The model developed by Lee and Green (2014) for WNA ranks first for a magnitude of 4.0 and 5.0 and also has good LLH values for a magnitude up to 7.0. However, for a magnitude of 8.0, the LLH value obtained is 8.44, which is higher compared to other models and is hence not recommended. A negative DSI value was also obtained for this magnitude which cross-verifies that this model is unsuitable. The model developed by Ghanat (2011) using data from the NGA database is excellent for magnitudes greater than 5.0 and will thus give accurate values for the duration

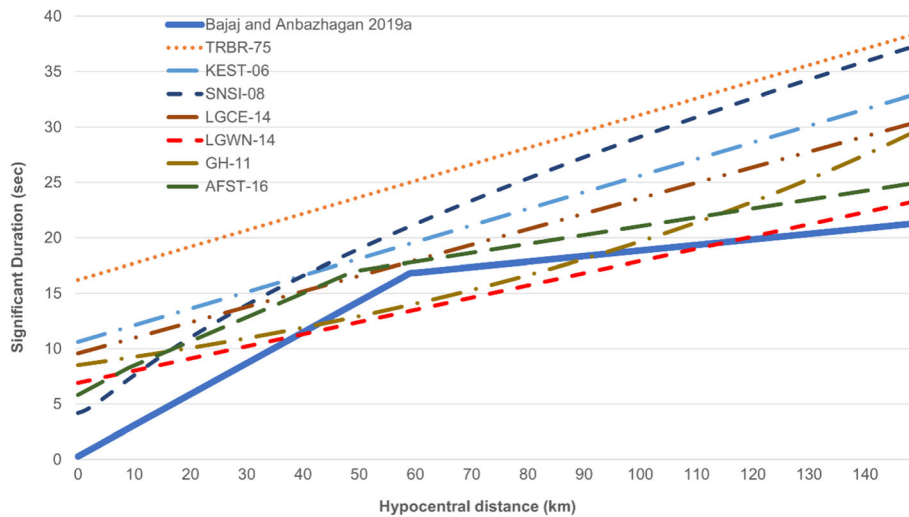


Figure 4. Graphical comparison for various duration models for a magnitude of 6.5 (hypocentral distance range 0–150 km).

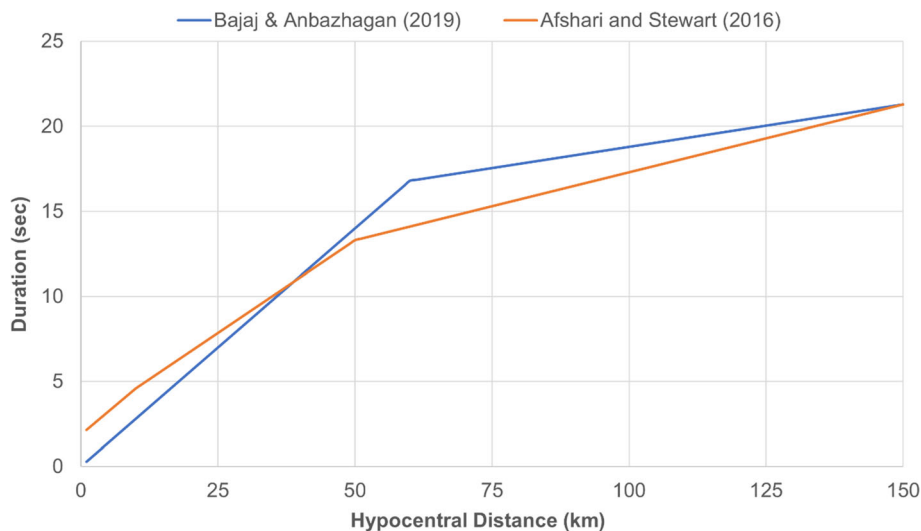


Figure 5. Comparison of the models developed by Bajaj and Anbazhagan (2019) with Afshari and Stewart (2016) for a moment magnitude of 5.0 at a distance of 0–150 km.

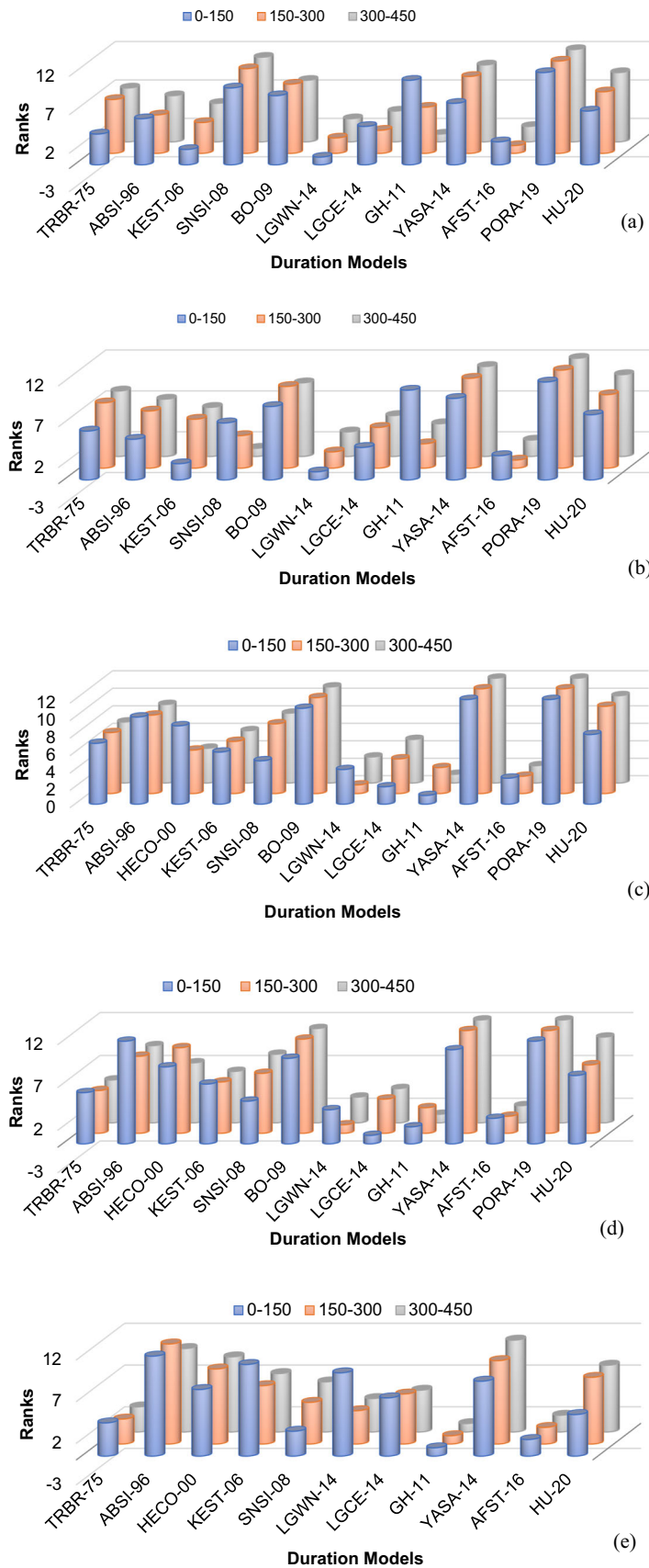


Figure 6. Ranking of various duration models for the 3 distance ranges considered. The models whose LLH values were undetectable have been excluded. Magnitude ranges considered (a) 4.0, (b) 5.0, (c) 6.5, (d) 7.0 and (e) 8.0.

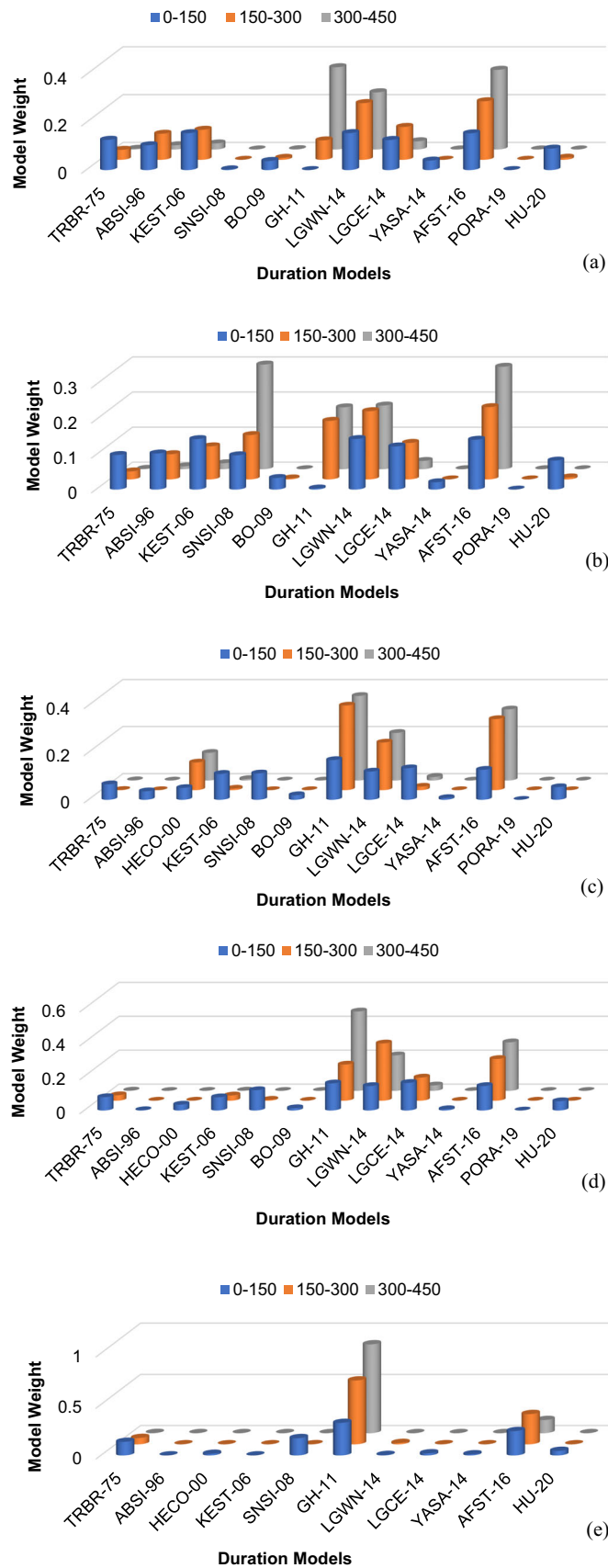


Figure 7. Graphical representation of the weights of different models for different hypocentral distance ranges. The models whose LLH values were undetectable have been excluded. Magnitude ranges considered (a) 4.0, (b) 5.0, (c) 6.5, (d) 7.0 and (e) 8.0.

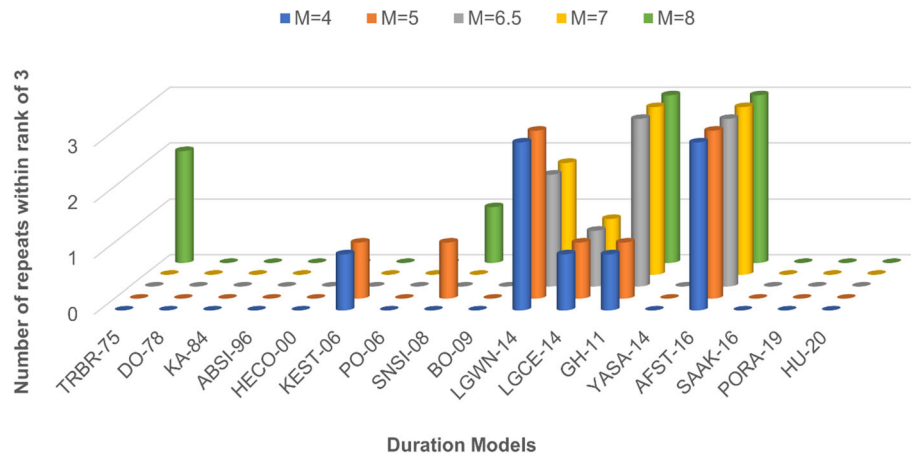


Figure 8. Graphical representation of the number of repeated ranks within the range of 3 for different magnitude ranges. We infer from this chart that Afshari and Stewart (2016) is the most suitable model for all the magnitude ranges.

for the Himalayan region. The model developed by Afshari and Stewart (2016) is very close to the reference model developed by Bajaj and Anbazhagan (2019) for all the magnitudes. A comparison of the two models is shown in figure 5 for a moment magnitude of 5.0.

The models developed by Dobry *et al.* (1978), Kamiyama (1984) and Sandikkaya and Akkar (2016) have very high LLH values in the 150–300 and 300–450 km range as well. Snæbjörnsson and Sigbjörnsson (2008) and Trifunac and Brady (1975) developed models with moderate LLH values, however, the ranking for these models amongst various magnitudes and hypocentral distance ranges is relatively higher. The model developed by Lee and Green (2014) for WNA has low values for magnitudes less than 6.5. However, for higher magnitudes, the hypothesis proposed by Ghanat (2011) shows the best values. The LLH values of the model developed by Ghanat (2011) for magnitudes greater than 6.5 in the 150–300 km range are not as low when compared to those in the range of 0–150 km. However, it is the best when compared to the other models. If one model is to be used for all magnitudes, the hypothesis proposed by Afshari and Stewart (2016) would be the most suitable.

For hypocentral distances in the range of 300–450 km, the model developed by Afshari and Stewart (2016) gives the most suitable values for magnitudes 4.0 and 5.0. The hypothesis by Ghanat (2011) has the best value for a magnitude of 4.0 but a relatively higher value for a magnitude of 5.0. For higher magnitudes, the model developed by Ghanat (2011) would be the best as it has top ranks in the magnitudes 6.5, 7.0, and 8.0. Figure 6 shows a graphical representation of these ranks. The

weights of each model have also been estimated for all distance ranges and are represented in figure 7. The model developed by Afshari and Stewart (2016) is the most consistent and coincidentally has a rank of two across all magnitudes. As one would expect, since the LLH values of this model are relatively low for most cases, their DSI values and corresponding weights are relatively higher. Figure 8 represents the number of times an LLH rank has been repeated within a threshold rank of 3. We observe from this chart that the hypothesis by Afshari and Stewart (2016) gives the highest return for not one but all magnitudes considered. This means that the rank of this model is within the top 3 ranks for all ranges of hypocentral distance for each of the considered magnitudes, clearly indicating the robustness of the equation. This model is also the only model that has positive DSI values for each range of hypocentral distance and all considered magnitudes. If a single model is to be used to estimate duration, the model developed by Afshari and Stewart (2016) would be most suitable. If multiple models are to be selected, we suggest using the model developed by Lee and Green (2014) for WNA for a magnitude up to 5.0 and the model by Ghanat (2011) for magnitudes above 5.0.

6. Summary and conclusion

Ground motion duration has a significant effect on the extent of damage to a structure. Presently, duration is not accounted for in the seismic resistance design of structures in India due to a lack of region-specific studies on duration and predictive models. This study presented suitable duration

models developed for different parts globally, considering data from past earthquakes. Different duration predictive models developed for the significant duration (D_{5-95}) are compared using the log-likelihood method. Log-likelihood value is estimated for each model and is used to rank all applicable models. This approach measures the distance between two continuous probability distribution functions. The LLH ranks, DSI values, and weights for all applicable models have been presented. Different models were recommended across various hypocentral distance ranges. However, the model developed by Afshari and Stewart (2016) using the NGA-West 2 database has been consistent across all 3 ranges of hypocentral distance and is hence highly recommended for duration estimation in the Himalayas. One must be very cautious in selecting the suitable model depending on the magnitude and hypocentral distance for appropriate duration estimation. Ground motion duration estimation can be further improved if a model is generated by incorporating significant data from the Himalayan region.

Acknowledgements

The authors thank the Dam Safety (Rehabilitation) Directorate, Central Water Commission for funding the project entitled ‘Capacity Buildings in Dam Safety’ under ‘Dam Rehabilitation and Improvement Project’. The authors would also like to thank the M/s Secon for funding the project ‘Effect of shear wave velocity calibration on amplification of shallow and deep soil sites’ Ref.: SECON/IISc/MoES/WO/07-18/0079, date: 14/8/2018.

Author statement

P Anbazhagan contributed to the methodology, conceptualization, envisioning the guided work and drafting of the manuscript. Kunal Motwani contributed to data collection, performing the analysis and drafting of the manuscript.

References

- Abrahamson N A and Silva W J 1996 *Empirical ground motion models*; Technical report 1996 Brookhaven National Laboratory.
- Afshari K and Stewart J 2016 Physically parameterized prediction equations for significant duration in active crustal regions; *Earthq. Spectra* **32**, <https://doi.org/10.1193/063015EQS106M>.
- Anbazhagan P, Sreenivas M, Ketan B and Sayed Sr Moustafa 2016 Selection of ground motion prediction equations for seismic hazard analysis of peninsular India; *J. Earthq. Eng.* **20** 699–737.
- Anbazhagan P, Neaz Sheikh M, Bajaj K, Mariya Dayana P J, Madhura H and Reddy G R 2017 Empirical models for the prediction of ground motion duration for intraplate earthquakes; *J. Seismol.* **21** 1001–1021, <https://doi.org/10.1007/s10950-017-9648-2>.
- Anbazhagan P, Joo M R, Rashid M M and Al-Arifi N S N 2021 Prediction of different depth amplifications of deep soil sites for potential scenario earthquakes; *Nat. Hazards*, pp. 1–29.
- Arias A 1970 Measure of earthquake intensity; In: *Seismic design for nuclear power plants* (ed.) Hansen R J, MIT Press, Cambridge, Massachusetts, pp. 438–483.
- Auden J B and Ghosh A M N 1934 Preliminary account of the earthquake of the 15th January, 1934, in Bihar and Nepal; *Rec. Geol. Surv. India* **68** 177–293.
- Bajaj K and Anbazhagan P 2019 Regional stochastic GMPE with available recorded data for active region – Application to the Himalayan region; *Soil Dyn. Earthq. Eng.* **126** 105825.
- Bommer J J and Martínez-Pereira A 1999 The effective duration of earthquake strong motion; *J. Earthq. Eng.* **3** 127–172, <https://doi.org/10.1080/13632469909350343>.
- Bommer J J, Hancock J and Alarcón J E 2006 Correlations between duration and number of effective cycles of earthquake ground motion; *Soil Dyn. Earthq. Eng.* **26** 1–13.
- Bommer J J, Stafford P J and Alarcón J E 2009 Empirical equations for the prediction of the significant, bracketed, and uniform duration of earthquake ground motion; *Bull. Seismol. Soc. Am.* **99** 3217–3233.
- Boore D and Thompson E 2014 Path durations for use in the stochastic-method simulation of ground motions; *Bull. Seismol. Soc. Am.* **104**, <https://doi.org/10.1785/0120140058>.
- Delavaud E, Scherbaum F, Kuehn N and Allen T 2012 Testing the global applicability of ground-motion prediction equations for active shallow crustal regions; *Bull. Seismol. Soc. Am.* **102** 707–721, <https://doi.org/10.1785/0120110113>.
- Dobry R, Idriss I M and Ng E 1978 Duration characteristics of horizontal components of strong-motion earthquake records; *Bull. Seismol. Soc. Am.* **68** 1487–1520.
- Douglas J 1964–2020 *Ground motion prediction equations*; Pacific Earthquake Engineering Research Center, Berkeley, CA.
- Ghanat S 2011 Duration characteristics of the mean horizontal component of shallow crustal earthquake records in active tectonic regions; Ph.D. Thesis, Arizona State University.
- Hernandez B and Cotton F 2000 Empirical determination of the ground shaking duration due to an earthquake using strong motion accelerograms for engineering applications; In: *Proceedings of Twelfth World Conference on Earthquake Engineering*.
- Huang C, Tarbali K and Galasso C 2020 Correlation properties of integral ground-motion intensity measures from Italian strong-motion records; *Earthq. Eng. Struct. Dyn.* **49** 1581–1598.

- Kamiyama M 1984 Effects of subsoil conditions and other factors on the duration of earthquake ground shakings; In: *Eighth World Conference on Earthquake Engineering*, Volume II, pp. 793–800.
- Kempton J J and Stewart J P 2006 Prediction equations for significant duration of earthquake ground motions considering site and near-source effects; *Earthq. Spectra* **22** 985–1013.
- Khatti K N 1987 Great earthquakes, seismicity gaps and potential for earthquake disaster along the Himalaya plate boundary; *Tectonophysics* **138** 79–92.
- Lee J and Green R 2014 An empirical significant duration relationship for stable continental regions; *Bull. Earthq. Eng.* **12**, <https://doi.org/10.1007/s10518-013-9570-0>.
- Podili B and Raghukanth S T G 2019 Ground motion prediction equations for higher order parameters; *Soil Dyn. Earthq. Eng.* **118** 98–110, <https://doi.org/10.1016/j.soildyn.2018.11.027>.
- Pousse G, Bonilla L F, Cotton F and Margerin L 2006 Nonstationary stochastic simulation of strong ground motion time histories including natural variability: Application to the K-net Japanese database; *Bull. Seismol. Soc. Am.* **96** 2103–2117, <https://doi.org/10.1785/0120050134>.
- Ramkrishnan R, Sreevalsa K and Sitharam T G 2019 Development of new ground motion prediction equation for the North and Central Himalayas using recorded strong motion data; *J. Earthq. Eng.* 1–24.
- Salmon M W, Short S A and Kennedy R P 1992 Strong motion duration and earthquake magnitude relationships; United States, <https://doi.org/10.2172/67453>.
- Sandikkaya M A and Akkar S 2016 Cumulative absolute velocity, Arias intensity and significant duration predictive models from a pan-European strong-motion dataset; *Bull. Earthq. Eng.*, pp. 1–18, <https://doi.org/10.1007/s10518-016-0066-6>.
- Scherbaum F, Delavaud E and Riggelsen C 2009 Model selection in seismic hazard analysis: An information-theoretic perspective; *Bull. Seismol. Soc. Am.* **99** 3234–3247.
- Sharma M L, Douglas J, Bungum H and Kotadia J 2009 Ground-motion prediction equations based on data from the Himalayan and Zagros regions; *J. Earthq. Eng.* **13** 1191–1210.
- Snæbjörnsson J and Sigbjörnsson R 2008 The duration characteristics of earthquake ground motions; In: *Proceedings of Fourteenth World Conference on Earthquake Engineering*.
- Trifunac M D and Brady A G 1975 A study on the duration of strong earthquake ground motion; *Bull. Seismol. Soc. Am.* **65** 581–626.
- Xie J, Wen Z and Li X 2012 Characteristics of strong motion duration from the Wenchuan Mw 7.9 earthquake; In: *Proceedings of the 15th World Conference on Earthquake Engineering*, Lisbon, Portugal.
- Yaghmaei-Sabegh S, Shoghian Z and Sheikh M N 2014 A new model for the prediction of earthquake ground-motion duration in Iran; *Nat. Hazards* **70** 69–92.

Corresponding editor: ANAND JOSHI